without K (fig. S4). This is another indication of NEA because K deposition onto a positive electron affinity semiconductor will lead to a shift of the low–kinetic energy cutoff and strong enhancement of the secondary electron background.

On a typical NEA surface, electrons excited into unoccupied states relax to the bottom of the conduction band as a result of inelastic scattering, a process normally referred to as the secondary cascade. A number of secondary electrons will then accumulate at the bottom of the conduction band. For a surface with positive electron affinity (as occurs in almost all untreated semiconductor surfaces), these accumulated electrons cannot escape. For an NEA surface, these accumulated electrons can be emitted directly because the vacuum level lies below the bottom of conduction band. As a result, a peak will be observed at the low–kinetic energy threshold in PES (*4*, *17–19*, *23*, *24*).

However, on diamondoid SAM surfaces, there is only a single layer of diamondoid molecules. The detailed mechanism responsible for the highly monochromatic emission is unknown at this stage. Naïvely, one may consider that photoexcited electrons lose energy by creating phonons in the molecules, but this would likely lead to the destruction of the molecules. A plausible scenario is that most of the photoexcited electrons come from the substrate. These electrons first thermalize in the metal, producing many more low-energy electrons. Electrons with energies above the diamondoid conduction-band minimum may get transferred to diamondoid molecules, reach the bottom of the conduction band by creating phonons, and get emitted. This proposal is shown schematically in Fig. 4. Another difference between our results and those of other typical NEA systems (*4*, *17–19*, *23*, *24*) is that our data show a spike in the spectra rather an exponential rise of the secondary tail toward the threshold, suggesting that a single energy level, resulting from the molecular nature of nanometer-sized diamondoids, and/or a strong resonance process are involved.

Our results suggest that diamondoid monolayers may have promising utility. Not only can functionalized diamondoids be easily grown into large area SAMs with NEA properties, they also naturally circumvent the long-standing electron-conductivity issues encountered for wide-gap bulk NEA semiconductors (*4*, *26*). On a diamondoid SAM surface, electron conduction from the electron reservoir (metal substrates) to the emission surface is through a single molecule, which successfully avoids the low-conductivity problem and enhances the electron emission. Additionally, the possibility of different functionalizations (*3*, *4*) allows one to optimize the NEA and other properties of diamondoids. Although many technical issues need to be addressed before diamondoid SAMs can be used as electron emitters, diamondoids provide intrinsic advantages over bulk materials because of their special molecular characteristics—for example, narrow energy distribution of the electronic states.

References and Notes

1. J. E. Dahl, S. G. Liu, R. M. K. Carlson, *Science* **299**, 96 (2003).
2. B. A. Tkachenko *et al.*, *Org. Lett.* **8**, 1767 (2006).
3. P. R. Schreiner *et al.*, *J. Org. Chem.* **71**, 8532 (2006).
4. A. Paoletti, A. Tucciarone, Eds., *The Physics of Diamond*, Proceedings of the International School of Physics Enrico Fermi (IOS Press, Amsterdam, 1997).
5. N. D. Drummond, A. J. Williamson, R. J. Needs, G. Galli, *Phys. Rev. Lett.* **95**, 096801 (2005).
6. Materials and methods are available as supporting material on *Science* Online.
7. A. Ulman, *Chem. Rev.* **96**, 1533 (1996).
8. J. Stöhr, *NEXAFS Spectroscopy* (Springer, Berlin, 1992).
9. G. Hähner, *Chem. Soc. Rev.* **35**, 1244 (2006).
10. M. Zharnikov, M. Grunze, *J. Phys. Condens. Matter* **13**, 11333 (2001).
11. T. M. Willey *et al.*, *Phys. Rev. Lett.* **95**, 113401 (2005).
12. T. M. Willey *et al.*, *Phys. Rev. B* **74**, 205432 (2006).
13. P. E. Laibinis *et al.*, *J. Am. Chem. Soc.* **113**, 7152 (1991).
14. A. Shaporenko *et al.*, *Langmuir* **21**, 4370 (2005).
15. J. C. Love *et al.*, *Chem. Rev.* **105**, 1103 (2005).
16. D. G. Castner, K. Hinds, D. W. Grainger, *Langmuir* **12**, 5083 (1996).
17. F. J. Himpsel, J. A. Knapp, J. A. VanVechten, D. E. Eastman, *Phys. Rev. B* **20**, 624 (1979).
18. B. B. Pate, *Surf. Sci.* **165**, 83 (1986).
19. J. van der Weide, R. J. Nemanich, *Appl. Phys. Lett.* **62**, 1878 (1993).
20. W. L. Yang *et al.*, *Science* **300**, 303 (2003).
21. C. D. Bain *et al.*, *J. Am. Chem. Soc.* **111**, 321 (1989).
22. The lack of a strong secondary electron component on the annealed sample may indicate that the transmission efficiency of the spectrometer is poor at low kinetic energies. This suggests that the peak from SAM surface could have been even stronger. Artificial effects on the peak have been ruled out by testing with different bias voltages.
23. L. W. James, J. L. Moll, *Phys. Rev.* **183**, 740 (1969).
24. R. C. Eden, J. L. Moll, W. E. Spicer, *Phys. Rev. Lett.* **18**, 597 (1967).
25. For NEA materials, the difference between photoemission spectral width and the excitation energy should match the band-gap value (*4*, *17–19*). Although there is no precise gap value reported for [121]tetramantane-6-thiol, and it is difficult to define a precise photoemission spectral width of an insulating monolayer system (owing to the difficulty in determining the spectral onset), the estimate obtained from our spectra is consistent with the DMC calculation (*5*), considering that the thiol groups are likely to change the gap value by only a few tenths of an electron volt.
26. R. L. Bell, *Negative Electron Affinity Devices* (Clarendon, Oxford, 1973).
27. We acknowledge helpful discussions with Z. Liu, D.-H. Lee, and H. Padmore. W.L.Y. thanks Y. Y. Wang for sharing information on diamondoid film deposition and J. Pepper and S. DiMaggio for technical support. The work at Stanford Synchrotron Radiation Laboratory and the Advanced Light Source is supported by the U.S. Department of Energy, Office of Basic Energy Science, Division of Material Science, under contracts DE-FG03-01ER45929-A001 and DE-AC03-765F00515, respectively. The work at Stanford is also supported by Chevron through the Stanford-Chevron Program on Diamondoid Nano-Science.

Coherence Dynamics in Photosynthesis: Protein Protection of Excitonic Coherence

Hohjai Lee, Yuan-Chung Cheng, Graham R. Fleming*

The role of quantum coherence in promoting the efficiency of the initial stages of photosynthesis is an open and intriguing question. We performed a two-color photon echo experiment on a bacterial reaction center that enabled direct visualization of the coherence dynamics in the reaction center. The data revealed long-lasting coherence between two electronic states that are formed by mixing of the bacteriopheophytin and accessory bacteriochlorophyll excited states. This coherence can only be explained by strong correlation between the protein-induced fluctuations in the transition energy of neighboring chromophores. Our results suggest that correlated protein environments preserve electronic coherence in photosynthetic complexes and allow the excitation to move coherently in space, enabling highly efficient energy harvesting and trapping in photosynthesis.

Highly efficient solar energy harvesting and trapping in photosynthesis relies on sophisticated molecular machinery built from pigment-protein complexes (*1*, *2*). Although the pathways and time scales of excitation energy

Department of Chemistry and QB3 Institute, University of California, Berkeley and Physical Bioscience Division, Lawrence Berkeley National Laboratory, Berkeley, CA 94720, USA.

*To whom correspondence should be addressed. E-mail: GRFleming@lbl.gov

transfers within and among these photosynthetic complexes are well studied, less is known about the precise mechanism responsible for the energy transfer. In particular, to what extent quantum coherence contributes to the efficiency of energy transfer is largely unknown. Only recently have nonlinear optical spectroscopy and theoretical modeling started to reveal that coherences between electronic excitonic states can have a substantial impact on excitation energy transfer in photosynthetic systems (*2–4*). For example,

Engel *et al.* have demonstrated using two-dimensional (2D) electronic spectroscopy that surprisingly long-lived (>660 fs) quantum coherences between excitonic states play an important role in the dynamics of energy transfer in photosynthetic complexes—i.e., the energy transfer is described by wavelike coherent motion instead of incoherent hopping (*4*).

To understand the origins of such long-lived coherences and the role of the protein matrix in its preservation, an experiment specifically designed to monitor electronic coherences between excited states is required. Here, we describe a two-color electronic coherence photon echo experiment (2CECPE) that produces a direct probe of electronic coherences between two exciton states. We applied the method to the coherence between bacteriopheophytin and accessory bacteriochlorophyll in the purple bacteria reaction center (RC). The measurement quantifies dephasing dynamics in the system and provides strong evidence that the collective long-range electrostatic response of the protein environment to the electronic excitations is responsible for the long-lasting quantum coherence. In other words, the protein environment protects electronic coherences and plays a role in the optimization of excitation energy transfer in photosynthetic complexes.
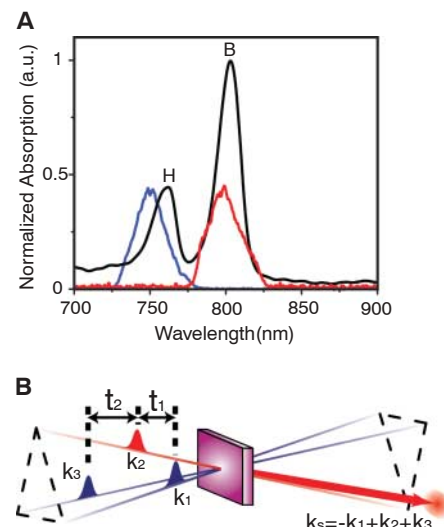
The RC from the photosynthetic purple bacterium *Rhodobacter sphaeroides* includes a bacteriochlorophyll dimer called the special pair (P) in the center, an accessory bacteriochlorophyll flanking P on each side (BChl; B_L and B_M, for the L and M peptides, respectively), and a bacteriopheophytin (BPhy; H_L and H_M for the L and M peptides, respectively) next to each BChl (*5*). (We use H and B to denote excitonic states whose major contributions are from monomeric BPhy and accessory BChl in the RC, respectively.) In addition to electron transfer with near-unity efficiency (*6*), energy transfer occurs between the excitonically coupled chromophores—for example, from H to B in about 100 fs and from B to P in about 150 fs—in the isolated RC (*7–10*). In our experiments, the primary electron donor (P) is chemically oxidized by $K_3Fe(CN)_6$ (*11*), which blocks electron transfer from P to H_L, but does not affect the dynamics of energy transfer (*8*). This modification eliminates interference from the charge-transfer dynamics. The absorption spectrum of the P-oxidized RC at 77 K (Fig. 1A) shows the H band at 750 nm and the B band at 800 nm.

In our 2CECPE (*11*) (Fig. 1B), three ~40-fs laser pulses interact with the sample and generate a signal field in the phase-matched direction k_s. The first two pulses have different colors and are respectively tuned for resonant excitation of the H transition at 750 nm and the B transition at 800 nm (Fig. 1A). This is different from conventional two-color three-pulse photon echo technique in which the first two pulses have the same color (*12*). In our experiment, the first pulse (750 nm) creates an optical coherence (electronic superposition) between the ground state and the H excitonic state ($|g\rangle\langle H|$ coherence). The coherence evolves for time delay t_1 until the second pulse (800 nm) interacts with the sample to form a coherence between B and H ($|B\rangle\langle H|$ coherence) that evolves for a time t_2. Finally, the third pulse (750 nm) interacts with the system to generate a photon echo signal if, and only if, B and H are mixed. The integrated intensity of the echo signal is recorded at different delay times t_1 and t_2. The central idea of the experiment is that if two chromophores are coupled and create two exciton bands (H and B in this case) in the absorption spectrum, then excitation resonant with one transition ($|g\rangle\rightarrow|H\rangle$), followed by excitation resonant with the other ($|g\rangle\rightarrow|B\rangle$) converts the initial coherence ($|g\rangle\langle H|$) into a coherence of the two exciton bands ($|B\rangle\langle H|$). This experiment is distinct from conventional two-color three-pulse photon echo measurements because different colors in the first two pulses are used to optically select the contributions to the third-order response function that arise from coherence pathways involving electronic superposition between two exciton states in the t_2 period. Because the system is in a coherence state in time t_2, population dynamics only contribute to dephasing and do not generate additional echo signals; therefore, this technique is specifically sensitive to the coherence dynamics and provides a probe for the protein environment of the chromophores. A similar pulse ordering was applied in dual-frequency 2D infrared spectroscopy to study vibrational coherence transfer and mode couplings (*13, 14*).

The 2CECPE signals for the RC as a function of t_1 and t_2 measured at 77 K and 180 K are shown in Fig. 2, A and B, respectively. These figures provide a 2D representation of the system, which propagates as a $|g\rangle\langle H|$ coherence during the t_1 period and as a $|B\rangle\langle H|$ coherence during the t_2 period. The result is a map showing the dephasing dynamics of the $|g\rangle\langle H|$ coherence along the t_1 axis and the dynamics of the $|B\rangle\langle H|$ coherence along the t_2 axis. Clearly, the decay of the $|g\rangle\langle H|$ coherence is much faster than the decay of the $|B\rangle\langle H|$ coherence. Moreover, following the black curve that connects the maximum of integrated echo signal at fixed t_2, we see that the signals exhibit a sawtooth-shaped beating pattern that persists for longer than $t_2 > 400$ fs. This oscillatory behavior is not from excitonic beating, given that we detect signal intensities in which the oscillatory phase factor vanishes; instead, this beating indicates electronic coupling to vibrational modes. Notably, the pattern is also peculiarly slanted along the antidiagonal direction; this slant arises because the vibrational coherence is induced by the first laser pulse and propagates in time $t_1 + t_2$, making the peaks of the beats parallel to the antidiagonal ($t_1 + t_2$ is fixed). The signals show substantial peak shift [i.e., shift from $t_1 = 0$ (*12*)], indicating correlation of the excitation energies between the H and B transitions (*12*).

To analyze the $|B\rangle\langle H|$ coherence dynamics, we plotted the integrated signal at $t_1 = 30$ fs (across the maxima of the first beat) as a function of t_2 (Fig. 3). Clearly, the dephasing is enhanced at higher temperature, as expected. The decay of the echo signal as a function of t_2 is not described by a single exponential decay because of its highly non-Markovian nature and the vibrational modulation. A Gaussian-cosine fit of the signal shows that the main component of the coherence signal decays with a Gaussian decay time (τ_g) of 440 and 310 fs at 77 and 180 K, respectively (eq. S1 and fig. S1). These dephasing times are substantially longer than the experimentally estimated excitation energy transfer time scale of about 250 fs from H to B to P^+ (*8*). The surprisingly long-lived $|B\rangle\langle H|$ coherence indicates that the excitation energy transfer in the RC cannot be described by Förster theory, which neglects the coherence between donor and acceptor states (*15*). In addition, the decay of the $|g\rangle\langle H|$ coherence is much faster than the decay of the $|B\rangle\langle H|$ coherence. Considering that the dephasing of the $|g\rangle\langle H|$ coherence is caused by the transition energy fluctuations on H, whereas the dephasing of the $|B\rangle\langle H|$ coherence is due to the fluctuations on the gap between H and B transition energies, the transition energy fluctuations on B and H must be strongly correlated, because in-phase energy fluctuations do not destroy coherence. Such a strong correlation can arise for two possible reasons: strong electronic coupling between B and H and/or strong correlation between nuclear modes that modulate transition frequency fluctuations of localized BChl and

A

B

Fig. 1. The 2CECPE experiment. (**A**) The 77 K absorption spectrum (black) of the P-oxidized RC from the photosynthetic purple bacterium *R. sphaeroides* and the spectral profiles of the ~40-fs laser pulses (blue, 750 nm; red, 800 nm) used in the experiment. (**B**) The pulse sequence for the 2CECPE experiment. We detect the integrated intensity in the phase-matched direction $k_s = -k_1 + k_2 + k_3$. a.u., arbitrary units.

BPhy excitations. Our theoretical analysis found that strong electronic coupling alone cannot re-produce the sawtooth pattern and a dephasing time as long as that observed (*11*). Instead, cross-correlation between nuclear modes modulating the energy levels of localized BChl and BPhy excitations is required.

We modeled the 2CECPE signals using im-pulsive limit third-order response functions for a coupled heterodimer based on the transition fre-quency correlation functions for each localized excitation (*11*, *16*). The model correlation func-tions contain a sum of a Gaussian component representing solvent reorganization and a con-stant term representing the inhomogeneous static contribution:

$$C_i(t) = \langle \Delta\omega_i^2 \rangle \exp(-t^2/\tau_i^2) + \Delta_i^2 \quad (1)$$

where $\langle \Delta\omega^2 \rangle^{1/2}$ is the fluctuation amplitude that is determined by the reorganization energy λ, τ is the bath relaxation time, Δ is the standard de-viation of Gaussian static distribution, and $i = h$, b, and hb denote the localized BPhy, BChl exci-tations, and the cross-correlation between them, respectively. For $C_h(t)$ and $C_b(t)$, we adopted parameters established by previous photon echo experiments on the neutral RC and by quantum chemistry calculations (*17–20*). For simplicity, we used a single coefficient c to describe the cross-correlation and assume $\lambda_{hb} = c \cdot \sqrt{\lambda_h \lambda_b}$ and $\Delta_{hb}^2 = c \cdot \Delta_h \Delta_b$. The cross-correlation coefficient c represents the extent to which nuclear motions modulating the transition frequencies of localized BPhy and BChl excitations are correlated with

each other. With $c = 0.9$ and the addition of a vibrational mode coupled to the localized BPhy excitation ($\omega = 250$ cm^{-1}; Huang-Rhys factor $S = 0.4$; damping time > 0.6 ps; phase shift 0.28 rad), the model semiquantitatively reproduces the measurements at 77 and 180 K simultaneously; a c value of 0.6 substantially diminishes agree-ment with experiment (Figs. 2 and 3). Adding more terms to the model correlation functions improves the fit to experiments, but does not change any conclusions.

A c value near unity implies that nuclear modes coupled to H and B exhibit almost iden-tical motions immediately after excitation. In other words, the two chromophores, H and B, are effectively embedded in the same protein envi-ronment and feel a similar short-time Gaussian component of their energy-level fluctuations. Most likely, this short-time component is the electrostatic response of the protein environment to the electronic excitations. Molecular dynamics simulations of the RC support this conclusion and show that interactions with the solvent en-vironment (protein and water), rather than the intramolecular contributions, dominate the tran-sition energy fluctuations of the P dimer excited state (*21*).

Theories for excitation energy transfer in pigment-protein complexes usually assume an independent bath for each of the individual chro-mophores (*1–3*, *15*, *22*, *23*). However, our result suggests that in densely packed pigment-protein complexes, the assumption of independent bath environments for each site is not correct. Indeed, a previous molecular dynamics simulation on the

RC of *Rhodopseudomonas viridis* also showed that nuclear motions of adjacent chromophores are strongly correlated (*24*). Given that closely packed pigment-protein complexes are a ubiqui-tous configuration for efficient energy harvesting and trapping in photosynthetic organisms, the long-range correlated fluctuations indicated by our results are unlikely to be unique.

What are the likely consequences of long-lived electronic coherence in the RC? First, such coherence enables the excitation to move rapidly and reversibly in space, allowing a very efficient search for the energetic trap, in this case the primary electron donor, P. The almost complete correlation of the H and B fluctuations (on the few hundred–femtosecond time scale) and the likely significant correlation of the fluctuations of both exciton states of P with those of B will also enable bath-induced coherence transfers between the various pairs of excitons (*25–27*). We suggest that the overall effect of the protection of electronic coherence is to substantially enhance the energy transfer efficiency for a given set of electronic couplings over that obtainable when electronic dephasing is fast compared with transfer times.

It will be important to confirm this proposal by carrying out experiments similar to the one described here, but with excitation wavelengths resonant with B and P and with H and P. The
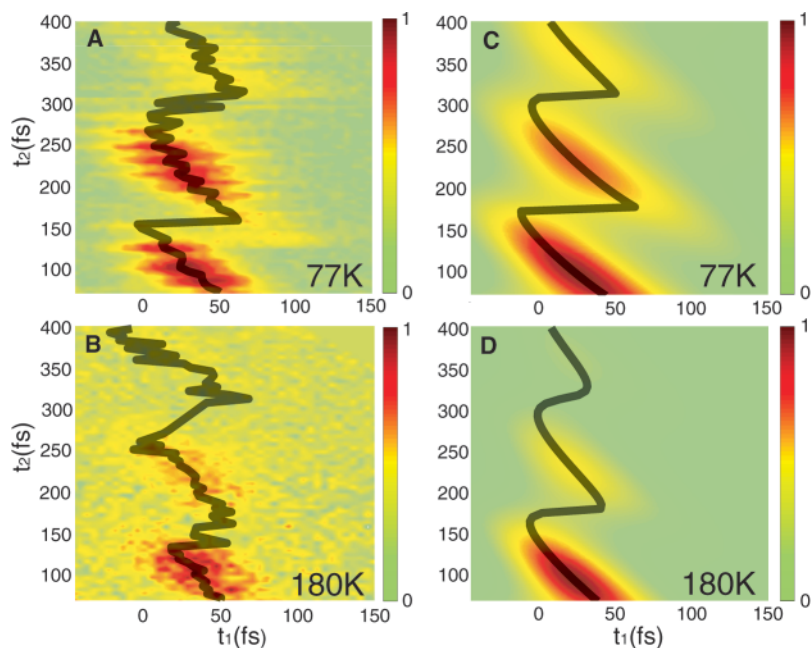
Fig. 2. Two-dimensional maps of experimental (**A** and **B**) and simulated (**C** and **D**) integrated echo signals as a function of the two delay times, t_1 and t_2, from the RC. The black lines follow the maximum of the echo signal at a given t_2. The data at $t_2 < 75$ fs are not shown because the conventional two-color three-pulse photon echo signal (750-750-800 nm) overwhelms the 2CECPE signal in this region, due to the pulse overlap effect.
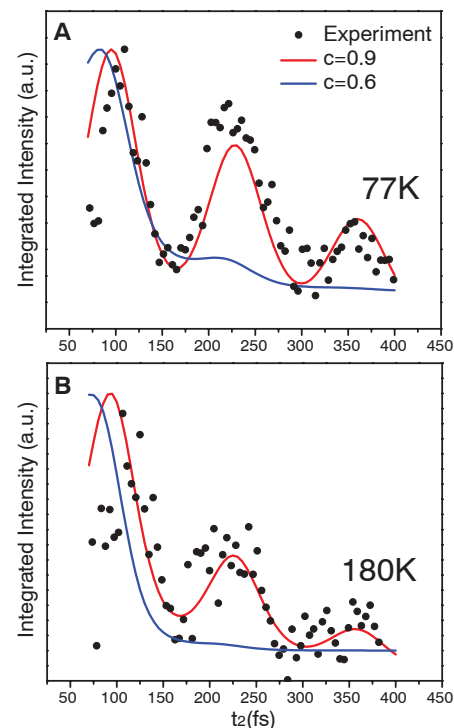
Fig. 3. Integrated echo signals as a function of t_2 at $t_1 = 30$ fs. Because the system evolves as a coherence between the H and B excitons during the t_2 period, this plot represents the dephasing dynamics of the |B⟩⟨H| coherence. Measurements at 77 K (**A**) and 180 K (**B**) are shown in solid circles, and the theoretical curves are shown in red ($c = 0.9$) or blue ($c = 0.6$) lines. a.u., arbitrary units.

recent results of Engel *et al.* on the Fenna-Matthew-Olson complex of green sulfur bacteria also suggest strong correlations between the fluctuations of the neighboring one-exciton states of the complex (*4*). Clearly, further studies are required before it can be stated that correlated fluctuations and the consequent protection of electronic coherence is a general feature of photosynthetic pigment-protein complexes, but it seems clear that any accurate description of the dynamics (and design principles) of these systems will require proper consideration of both quantum coherences and long-range system-bath interactions (*3, 22, 23*).

We close by briefly comparing the present technique with existing experimental methods. In principle, 2D electronic spectroscopy (*4, 28, 29*) and pump-probe anisotropy spectroscopy (*10, 23, 30*) both contain information about coherence dynamics in the form of quantum beatings. However, interferences from other coherence states and population relaxation can create a complicated beating pattern that makes a quantitative analysis of coherence dynamics in the 2D spectrum or an anisotropy decay difficult. In this regard, the 2CECPE technique provides a unique tool that can resonantly select third-order response contributions from a specific coherence pathway and should lead to a much-improved understanding of coherence dynamics and the protein fluctuations that govern these dynamics.

References and Notes

1. R. E. Blankenship, *Molecular Mechanisms of Photosynthesis* (Blackwell Science, Oxford, 2002).
2. R. van Grondelle, V. I. Novoderezhkin, *Phys. Chem. Chem. Phys.* **8**, 793 (2006).
3. O. Kühn, V. Sundström, T. Pullerits, *Chem. Phys.* **275**, 15 (2002).
4. G. S. Engel *et al.*, *Nature* **446**, 782 (2007).
5. U. Ermler, G. Fritzsch, S. K. Buchanan, H. Michel, *Structure* **2**, 925 (1994).
6. C. A. Wraight, R. K. Clayton, *Biochim. Biophys. Acta* **333**, 246 (1973).
7. R. J. Stanley, B. King, S. G. Boxer, *J. Phys. Chem.* **100**, 12052 (1996).
8. J. A. Jackson *et al.*, *J. Phys. Chem. B* **101**, 5747 (1997).
9. M. H. Vos, J. Breton, J.-L. Martin, *J. Phys. Chem. B* **101**, 9820 (1997).
10. D. C. Arnett, C. C. Moser, P. L. Dutton, N. F. Scherer, *J. Phys. Chem. B* **103**, 2014 (1999).
11. Materials and methods are available as supporting material on *Science* Online.
12. R. Agarwal, B. S. Prall, A. H. Rizvi, M. Yang, G. R. Fleming, *J. Chem. Phys.* **116**, 6243 (2002).
13. M. A. Rickard, A. V. Pakoulev, K. Kornau, N. A. Mathew, J. C. Wright, *J. Phys. Chem. A* **110**, 11384 (2006).
14. I. V. Rubtsov, J. Wang, R. M. Hochstrasser, *Proc. Natl. Acad. Sci. U.S.A.* **100**, 5601 (2003).
15. S. J. Jang, M. D. Newton, R. J. Silbey, *Phys. Rev. Lett.* **92**, 218301 (2004).
16. T. Meier, V. Chernyak, S. Mukamel, *J. Chem. Phys.* **107**, 8759 (1997).
17. M. L. Groot, J. Y. Yu, R. Agarwal, J. R. Norris, G. R. Fleming, *J. Phys. Chem. B* **102**, 5923 (1998).
18. X. J. Jordanides, G. D. Scholes, W. A. Shapley, J. R. Reimers, G. R. Fleming, *J. Phys. Chem. B* **108**, 1753 (2004).
19. D. Y. Parkinson, H. Lee, G. R. Fleming, *J. Phys. Chem. B* 10.1021/jp070029q (2007).
20. We used $\lambda_h = 50$ cm^{-1}, $\lambda_b = 80$ cm^{-1}, $\tau_h = \tau_b = 60$ fs, and $\Delta_h = \Delta_b = 20$ cm^{-1}, and we assumed the electronic coupling $J = 220$ cm^{-1} and the gap between excitonic H and B states is 680 cm^{-1}; these values are well within the range suggested by other theoretical studies and our recent experiments (*16–19*).
21. M. Souaille, M. Marchi, *J. Am. Chem. Soc.* **119**, 3948 (1997).
22. T. Renger, V. May, O. Kühn, *Phys. Rep.* **343**, 137 (2001).
23. V. Novoderezhkin, M. Wendling, R. van Grondelle, *J. Phys. Chem. B* **107**, 11534 (2003).
24. H. Treutlein *et al.*, *Proc. Natl. Acad. Sci. U.S.A.* **89**, 75 (1992).
25. P. de Bree, D. A. Wiersma, *J. Chem. Phys.* **70**, 790 (1979).
26. Y. Ohtsuki, Y. Fujimura, *J. Chem. Phys.* **91**, 3903 (1989).
27. J. M. Jean, G. R. Fleming, *J. Chem. Phys.* **103**, 2092 (1995).
28. T. Brixner, T. Mančal, I. V. Stiopkin, G. R. Fleming, *J. Chem. Phys.* **121**, 4221 (2004).
29. A. V. Pisliakov, T. Mančal, G. R. Fleming, *J. Chem. Phys.* **124**, 234505 (2006).
30. K. Wynne, R. M. Hochstrasser, *Chem. Phys.* **171**, 179 (1993).
31. This work was supported by the Office of Basic Energy Sciences, Chemical Sciences Division, U.S. Department of Energy (contract DE-AC03-76SF000098). We thank S. G. Boxer for *R. sphaeroides* samples; B. S. Prall and D. Y. Parkinson for valuable discussions; and E. A. Berry, L. S. Huang, and N. G. Pon for help with sample preparation.

Stepwise Quenching of Exciton Fluorescence in Carbon Nanotubes by Single-Molecule Reactions

Laurent Cognet,[1,2]* Dmitri A. Tsyboulski,[2]† John-David R. Rocha,[2]† Condell D. Doyle,[2] James M. Tour,[2] R. Bruce Weisman[2]*

Single-molecule chemical reactions with individual single-walled carbon nanotubes were observed through near-infrared photoluminescence microscopy. The emission intensity within distinct submicrometer segments of single nanotubes changed in discrete steps after exposure to acid, base, or diazonium reactants. The steps were uncorrelated in space and time and reflected the quenching of mobile excitons at localized sites of reversible or irreversible chemical attack. Analysis of step amplitudes revealed an exciton diffusional range of about 90 nanometers, independent of nanotube structure. Each exciton visited about 10,000 atomic sites during its lifetime, providing highly efficient sensing of local chemical and physical perturbations.

Optical excitation of semiconducting single-walled carbon nanotubes (SWNTs) generates relatively strongly bound excitons whose spatial dimensions are predicted to be a few nanometers (*1–3*). Experimental evidence of efficient exciton-exciton annihilation in nanotubes indicates that SWNT excitons have substantial mobility along the tube axis (*4–6*). However, the extent of this mobility is still experimentally and theoretically uncertain. A notable related effect is the strong suppression of photoluminescence (PL) when SWNT sidewalls are perturbed by chemical reactions (*7–9*). This quenching phenomenon has hampered the use of covalently derivatized SWNTs as near-infrared (near-IR) fluorophores.

We report the use of single-nanotube microscopy to detect stepwise changes in SWNT PL intensity within segments of individual nanotubes while they are exposed to chemical reactants. These stepwise changes in PL intensity are caused by reactions of single molecules with one nanotube. Since the pioneering low-temperature experiments of Orrit and Moerner, single-molecule

spectroscopy has proven to be a powerful tool that bypasses ensemble averaging in the study of static and dynamic nano-objects in various environments (*10, 11*). Single-molecule approaches are especially appealing for SWNT fundamental studies and applications (*12–14*) because the bulk samples are highly heterogeneous. In the present work, the magnitudes of PL intensity steps caused by single-molecule reactions reveals that the exciton excursion range in highly luminescent SWNTs is ~90 nm and is essentially independent of nanotube structure. This room-temperature excitonic motion is deduced to be diffusional. Because each nanotube exciton visits a very large number of atomic sites during its lifetime, PL quenching provides an ultrasensitive method for sensing and studying certain types of chemical reactions with nanotube sidewalls at the single-molecule level.

Our studies required highly luminescent and relatively long nanotubes that were immobilized yet accessible to added reactant solutions. We therefore used very brief tip ultrasonication to

[1]Centre de Physique Moléculaire Optique et Hertzienne, Université Bordeaux 1, and CNRS, Talence F-33405, France. [2]Department of Chemistry, Center for Biological and Environmental Nanotechnology, and R. E. Smalley Institute for Nanoscale Science and Technology, Rice University, Houston, TX 77005, USA.

*To whom correspondence should be addressed. E-mail: lcognet@u-bordeaux1.fr (L.C.); weisman@rice.edu (R.B.W.) †These authors contributed equally to this work.